

Microphysical properties of Antarctic polar stratospheric clouds and their dependence on tropospheric cloud systems

Loknath Adhikari,¹ Zhien Wang,¹ and Dong Liu^{1,2}

Received 26 March 2009; revised 16 November 2009; accepted 25 November 2009; published 8 April 2010.

[1] Cloud-Aerosol Lidar and Infrared Pathfinder Satellite Observation (CALIPSO) and CloudSat satellite measurements are used to investigate the impact of tropospheric high and deep clouds on the microphysical properties of polar stratospheric clouds (PSCs) over Antarctica during the 2006 and 2007 winters. Based on the attenuated lidar scattering ratio and PSC depolarization ratio (δ'), PSCs are classified into supercooled ternary solution (STS), Mix 1, Mix 2, and ice classes with significantly different microphysical properties in terms of the PSC backscattering coefficient (β_{532}) for 532 nm, the color ratio (β_{1064}/β_{532}), and δ' . In the early stages of the PSC season, STS accounts for more than 50% of the total PSCs, but the Mix 1, Mix 2, and ice classes become more common in the late season. During the late PSC season, close to 70% of PSCs are formed in association with high and deep tropospheric cloud systems, indicating the important role of tropospheric weather systems in Antarctic PSC formation. Tropospheric cloud systems also affect the microphysical properties of PSCs by affecting the relative occurrence of different PSC classes, especially during September and October. Our results also show that there are noticeable differences in color ratio and β_{532} (at the 0.05 significance level) for the ice class and Mix 2 (late season only) for PSCs associated and not associated with high and deep tropospheric cloud systems. These results indicate that the impact of tropospheric meteorology on PSC formation should be fully considered to better understand interannual variations and recovery of the Antarctic ozone hole.

Citation: Adhikari, L., Z. Wang, and D. Liu (2010), Microphysical properties of Antarctic polar stratospheric clouds and their dependence on tropospheric cloud systems, *J. Geophys. Res.*, 115, D00H18, doi:10.1029/2009JD012125.

1. Introduction

[2] Polar Stratospheric Clouds (PSCs) are important to ozone-depleting processes in the polar regions [Solomon, 1999; Tolbert and Toon, 2001; Rex et al., 2004; Douglass et al., 2006]. PSCs affect ozone depletion in two ways: (1) PSCs provide a surface for heterogeneous reactions that convert stable chlorine to highly reactive forms and nitrogen oxides to nitric acid [Strawa et al., 2002]. The reactive chlorine destroys ozone under sunlit conditions [Solomon, 1999; Hopfner et al., 2006]. (2) PSC particles containing nitric acid sediment out, causing denitrification of the stratosphere [Gobbi et al., 1998; Tabazadeh et al., 2001, Jensen et al., 2002]. Stratospheric nitrogen compounds react chemically to convert reactive chlorine to an inert form. Permanent removal of nitric acid through denitrification of the stratosphere prevents the formation of inert chlorine compounds and increases ozone destruction.

[3] Our current understanding of PSCs is based on laboratory investigations [Hanson and Mauersberger, 1988; Chu et al., 1993; Tabazadeh et al., 2000; Voigt et al., 2000], in situ measurements [Larsen et al., 2000; Drdla et al., 1994], modeling [Tabazadeh et al., 1994; Svendsen et al., 2005] and remote sensing [Fromm et al., 1997, 1999, 2003; Teitelbaum et al., 2001; Spang et al., 2005]. Recent advancements in satellite remote sensing using space-based lidars have greatly increased our potential to understand PSCs because these space-based lidars overcome the shortcomings of both limb measurements [Fromm et al., 2003; Spang et al., 2005] and surface-based lidar measurements [Adriani et al., 2004]. Space-based lidars have better horizontal and vertical resolution than limb measurements and provide better spatial coverage than surface lidars [Pitts et al., 2007; Noel et al., 2008; Wang et al., 2008]. Additionally, signal attenuation by tropospheric clouds, a major setback encountered in studying PSCs using surface-based lidars, is not an issue for space-based measurements. The NASA A-Train constellation that includes Cloud-Aerosol Lidar and Infrared Pathfinder Satellite Observations (CALIPSO) [Winker et al., 2003] and CloudSat [Stephens et al., 2002] satellites carry a depolarization-capable dual wavelength lidar, Cloud-Aerosol Lidar with Orthogonal Polarization (CALIOP) and a 94 GHz Cloud Profiling Radar (CPR), respectively. The

¹Department of Atmospheric Science, University of Wyoming, Laramie, Wyoming, USA.

²Key Laboratory of Atmospheric Composition and Optical Radiation, Chinese Academy of Sciences, Hefei, China.

different sensitivities of lidar and radar measurements to particle concentration and size distribution provide information for characterizing tropospheric cloud systems as well as PSCs. By combining other A-train satellite measurements, we have unique data that may allow for a better understanding of PSCs.

[4] Stratospheric air is characterized by a very low abundance of water vapor and nitric acid vapors, the major components of PSCs. Thus, low temperatures are required for the formation of cloud particles in the lower stratosphere. The Antarctic winter season, which is devoid of sunlight, provides suitable conditions for the occurrence of very low stratospheric temperatures. Moreover, the Antarctic stratosphere is strongly controlled by the polar vortex [World Meteorological Organization, 2007], which inhibits mixing of the polar stratospheric air with warmer low-latitude air, keeping the Antarctic stratosphere cooler. Three main types of PSCs have been observed, containing water, nitric acid and sulfuric acid in different proportions [Browell *et al.*, 1990; Carslaw *et al.*, 1994; Benson *et al.*, 2006; Lowe and MacKenzie, 2008]. Type Ia PSCs contain hydrates of nitric acid, predominantly nitric acid trihydrate (NAT) [Worsnop *et al.*, 1993; Tabazadeh *et al.*, 1994; Del Negro *et al.*, 1997; Strawa *et al.*, 2002]. Type Ib contains supercooled ternary solution (STS) [Toon *et al.*, 1990], and Type II particles are dominated by ice particles.

[5] The association of PSCs with tropospheric meteorology has been recognized previously, e.g., by Teitelbaum *et al.* [2001]. Teitelbaum *et al.* [2001] used Polar Ozone and Aerosol Measurement (POAM II) and Television Infrared Observation Satellites (TIROS) Operational Vertical Sounders (TOVS) data and showed that PSCs and ozone minima over the Arctic are associated with anticyclonic potential vorticity anomalies near the tropopause, resulting in an upward displacement of isentropic surfaces. The flow anomalies result in quasi-adiabatic uplift through the lower stratosphere, causing adiabatic cooling in the stratosphere. Similarly, Wang *et al.* [2008] showed that 66% of the PSCs over west Antarctica and 52% of the PSCs over east Antarctica were associated with deep tropospheric clouds during June through October 2006, based on CloudSat and CALIPSO observations. Local cooling associated with tropospheric synoptic or mesoscale events can provide suitable conditions for PSC formation; however, the extent to which tropospheric meteorology or tropospheric cloudiness affects PSCs is not well realized or understood. Perturbations in the local temperature field caused by tropospheric cloud systems may also affect PSC microphysical properties. Using the CALIPSO and CloudSat measurements, this study explores the effects of tropospheric cloud systems on the microphysical properties of PSCs. Section 2 gives details of the data used and the methodology applied. Section 3 details the results from the study, and section 4 provides conclusions drawn from the study.

2. Data Analysis

2.1. PSC and Tropospheric Cloud Detection

[6] CALIPSO and CloudSat measurements taken during the periods of June through October 2006 and May through October 2007 are used in this study. Temperature mea-

surements for the same periods from the microwave limb sounder (MLS) on the Aura satellite are used as well.

[7] CALIPSO level 1B data are used for the detection of tropospheric clouds and PSCs and for the analyses of the microphysical properties of PSCs. CALIPSO level 1B data with vertical resolutions of 30 and 60 m in the ranges of -0.5 – 8.2 and 8.2 – 20.2 km are averaged to 180 m, the same as the vertical resolution within the range of 20.2 – 30.1 km. Then, CALIPSO profiles are collocated to the CloudSat footprint (1.4 km cross track \times 1.8 km along track) and averaged to form a collocated CALIPSO and CloudSat data set at a CloudSat horizontal resolution of 1.1 km for tropospheric cloud and PSC analyses. CloudSat radar bins with cloud mask values ≥ 30 in the CloudSat 2B-GEOPROF product are used to identify cloudy bins from radar measurements. Attenuated lidar scattering ratios (ALSR) calculated from CALIPSO measurements are also used to identify tropospheric clouds. The ALSR is the ratio of the total attenuated backscattering signal to the molecular-only attenuated backscattering signal. Molecular backscattering and the extinction coefficients are determined by the molecular number density profile calculated with the Geostationary Operational Environmental Satellite (GOES-4) temperature and pressure profiles included in the CALIPSO level 1B product. Simple threshold values of ALSR are used to identify tropospheric cloud boundaries for each averaged CALIPSO lidar profile, as described by Wang *et al.* [2008]. For cases in which there is no gap between the PSCs and the tropospheric clouds, the tropospheric cloud top is determined as the level at which the ALSR decreases below 4 and the ALSR for a height ~ 900 m lower exceeds 8. Due to different sensitivities and attenuation of the CloudSat radar and CALIPSO lidar measurements, the CloudSat and CALIPSO cloud masks are combined to provide tropospheric cloud structures over the Antarctic region south of 60°S .

[8] For the identification of PSCs, a threshold method similar to that of Pitts *et al.* [2007] is used. The collocated CALIPSO data is further moving-averaged to a horizontal resolution of 20 km to improve the signal-to-noise ratio for the ALSR. For nighttime measurements, vertical bins above 12 km and above tropospheric cloud tops with ALSR values above 1.8 are identified as PSCs; however, for daytime measurements, the ALSR threshold is set to 4 to exclude the effect of solar noise. Due to our choice of ALSR threshold, optically thin PSCs may be overlooked in our analysis. Pitts *et al.* [2009] showed an improved detection sensitivity for these optically thin PSCs with the addition of depolarization measurements that results in an increase of 15% in the areal coverage. These optically thin PSCs have a much smaller number concentration and small surface area as compared with PSC with ALSRs larger than 1.8, if we assume that they have a similar effective size. Therefore, the overall impact of missed optically thin PSCs on heterogeneous chemistry is small. Furthermore, these optically thin PSCs may or may not be associated with tropospheric cloud systems. Considering these points, we do not think that neglecting these thin PSCs will affect our conclusion. Figure 1 shows an example of our PSC detection algorithm and the classification scheme applied to data for 25 June 2006. CALIPSO 532 nm total attenuated backscattering coefficients ($\text{km}^{-1} \text{sr}^{-1}$, Figure 1a) together with CloudSat radar reflectivity

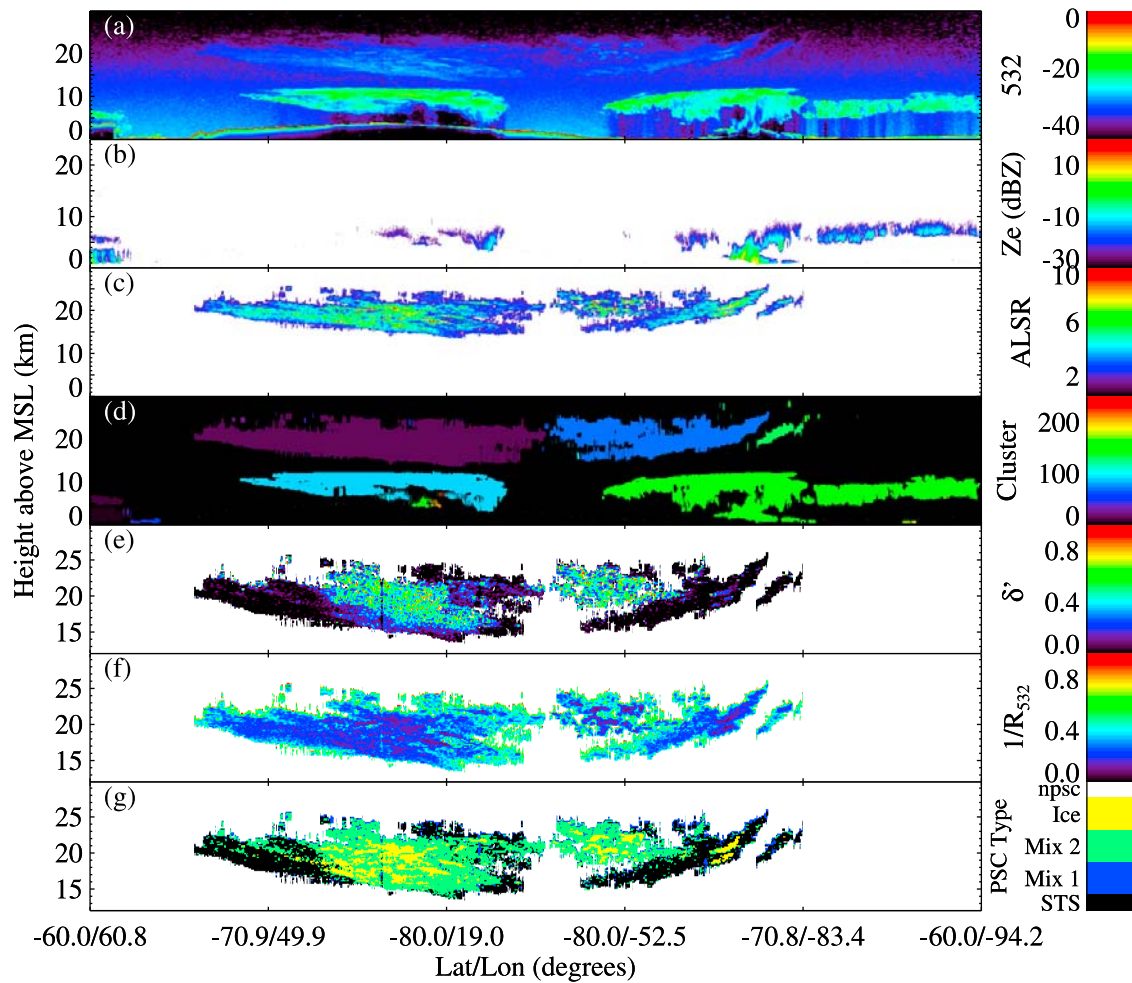


Figure 1. PSC identification and classification example based on 25 June 2006: (a) total attenuated backscattering coefficient at 532 nm, (b) radar reflectivity factor measured by CloudSat CPR, (c) ALSR within the PSCs, (d) clusters of PSCs and tropospheric cloud systems, (e) calculated PSC depolarization ratio (δ'), (f) inverse ALSR ($1/R_{532}$) for the PSCs, and (g) classification of different classes of PSCs based on Figures 1e and 1f.

factors (Figure 1b) show that tropospheric cloud systems extend up to 12 km above mean sea level (MSL). Figure 1c shows PSCs detected using the ALSR threshold method and their ALSR values. Horizontally and vertically connected tropospheric cloudy bins or PSC bins are identified and grouped together as a cluster (a single tropospheric cloud or PSC system). Figure 1d shows different identified tropospheric cloud and PSC clusters, each represented by a unique cluster number.

[9] To evaluate the effects of tropospheric clouds on PSCs, only high clouds (above 7 km) or deep clouds (depths greater than 6.5 km) are considered. If a PSC cluster is over a tropospheric cloud cluster associated with high and/or deep clouds, the PSC cluster could be impacted directly by the tropospheric system dynamically and radiatively, and we refer to this as a PSC cluster associated with a tropospheric cloud system. The areas of PSCs under the satellite track are calculated along the satellite track as the product of PSC thickness and along-track length.

2.2. PSC Optical and Microphysical Property Determination

[10] Analyses of PSC optical and microphysical properties are carried out by calculating the PSC depolarization ratio and the backscattering coefficient at 532 nm and the color ratio, the ratio of backscattering coefficients at the 1064 nm and 532 nm channels. Since we are interested in a possible connection of PSC microphysical properties with tropospheric cloud systems rather than the horizontal coverage of PSCs, we did not make any adjustment for the latitudinal nonuniformity of the CALIPSO/CloudSat data and weighted all measurements equally.

[11] Attenuated total backscattering (ATB) and perpendicular attenuated backscattering (PER) measurements are used to calculate the volume depolarization ratio (δ) given by

$$\delta = \frac{PER}{(ATB - PER)}. \quad (1)$$

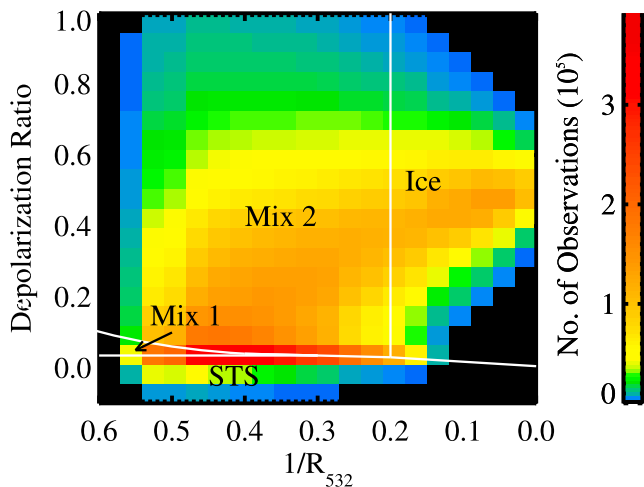


Figure 2. Classification of PSCs into four different class based on $1/\text{ALSR}$ and depolarization ratio values.

The effect of molecular scattering can be significant at 532 nm, especially at low ALSR values. To reduce the effect of molecular scattering, the PSC depolarization ratio (δ') is estimated with the following equation:

$$\delta' = \frac{(R\delta - \delta_m)}{(R + \delta_m - \delta - 1)}, \quad (2)$$

where R is the ALSR, and δ_m is the depolarization ratio for the molecular signal. In the present analysis, the value of δ_m is taken as 0.0035. δ' provides important information regarding the PSC phase.

[12] The PSC backscattering coefficient at 532 nm (β_{532}) can be estimated from 532 nm ATB by correcting for attenuation and then subtracting the molecular backscattering. PSC extinction can be estimated from the PSC backscattering coefficient by assuming a lidar ratio (extinction to backscatter ratio). By using the constraint of the PSC layer optical depth estimated with the molecular signals above and below the PSC layer, we found that the lidar ratios for PSCs mainly lie between 20 and 30. Thus, we used a mean lidar ratio of 25 to estimate the PSC extinction coefficients. The lidar ratio depends on PSC size and type, and the use of a single lidar ratio of 25 for all PSCs may result in large uncertainties for some cases. However, the impact on the estimated PSC backscattering is small because the optical depths of PSCs are small and the attenuation corrections are typically within 20% of ATB.

[13] The contribution of molecules to the 1064 nm measurements is negligible; thus, the total backscattering coefficient at 1064 nm (β_{1064}) can be regarded as PSC backscattering. We calculate the color ratio of PSC as $\text{CR}' = \frac{\beta_{1064}}{\beta_{532}}$. Although there are uncertainties in the absolute values of CR' due to calibration and attenuation correction errors, the relative change in CR' is still a good indicator for PSC effective particle size; that is, higher CR' values indicate PSCs with larger effective particle sizes. For PSCs with the same effective size, differences in the magnitude of β_{532} reflect differences in the PSC number concentrations.

2.3. PSC Composition Determination

[14] It is well established that PSCs are composed of solid crystalline particles and supercooled liquid solutions [Carlsaw *et al.*, 1994; Benson *et al.*, 2006]. Due to the different physical and optical characteristics of PSC particles, lidar depolarization measurements can be used to differentiate particle shapes to provide particle type information, e.g., Browell *et al.* [1990]. Type I PSCs form at higher temperatures [Strawa *et al.*, 2002] than Type II PSCs, which form when the temperature drops below the local frost point temperature. Type I PSCs are further classified into Types Ia and Ib, where Type Ia includes crystalline particles (mostly NAT) with diameters between 3 and 10 μm [Fahey *et al.*, 2001] and Type Ib consists of spherical supercooled liquid droplet STS. STS (Type Ib) particles consist of spherical liquid droplets and have very little perpendicular backscattering, which makes the depolarization ratio of STS very small. NAT particles, which are crystalline, have larger depolarization signals than STS. In the present analysis, the PSC classification scheme described by Pitts *et al.* [2009] is used. PSCs are classified into four classes, STS, Mix 1, Mix 2 and ice, according to the particle depolarization ratio and $1/\text{ALSR}$. Figure 2 shows the threshold values used to distinguish the four classes of PSCs and the distribution of PSCs observed in 2006. STSs are taken as those having depolarization ratio values between -0.03 and 0.035 . Mix 1 and Mix 2 are classified based on their ALSR values. Mix 2 represents an external mixture of different PSC particles that have a larger ALSR than Mix 1. Mix 1 also includes all PSCs with depolarization ratio values less than -0.03 (not shown in Figure 2). Ice includes PSCs with ALSR values above 5 ($1/\text{ALSR} < 0.2$) and depolarization ratio values larger than the threshold value used for STS, which depend on the ALSR values. Figures 1e and 1f show the particle depolarization ratio (δ') and $1/\text{ALSR}$ for the PSC identified in Figure 1c. Figure 1g shows the classification results.

3. Results and Discussion

3.1. Evolution of PSCs During the Winters of 2006 and 2007

[15] PSCs appear in the Antarctic stratosphere by late May and persist through late September/early October. They are ubiquitous in the Antarctic stratosphere during the southern hemisphere winter. Figure 3 shows monthly maps ($2.5^\circ \text{ lat} \times 5^\circ \text{ lon}$) of PSC occurrences calculated as the ratio of all of the profiles with PSCs to the total number of profiles in each grid for 2006 and 2007 between June and September. The monthly PSC maps reveal localized regions with high PSC occurrence. Figure 3 also shows a high spatial variability of PSC distribution among different months and between the two years. These localized regions of high PSC occurrences indicate the role of mesoscale dynamics in controlling the distribution of PSCs. Topographically forced mountain waves are known to be an important factor in PSC formation [Cariolle *et al.*, 1989; Carlsaw *et al.*, 1998]. They contribute to PSC formation by adiabatically cooling the stratosphere. Hopfner *et al.* [2006] showed, using limb measurements from Michaelson Interferometer for Passive Atmospheric Sounding (MIPAS), that PSCs formed by these topographically forced mountain waves can cover large areas and

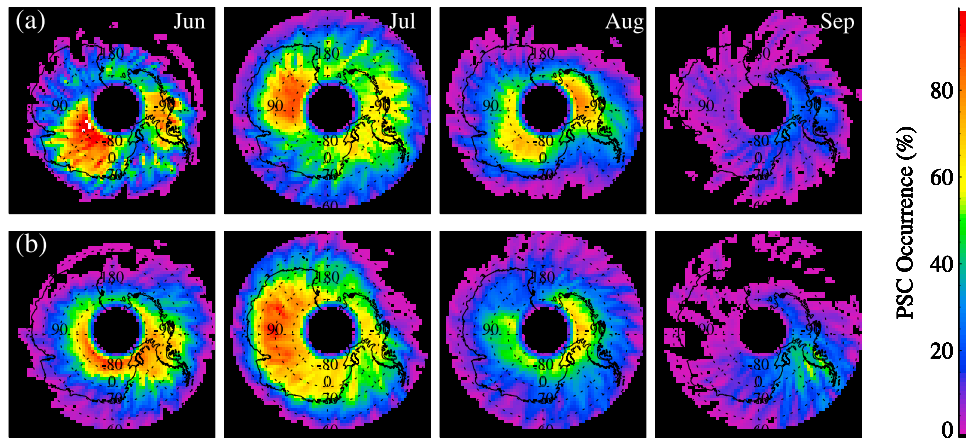


Figure 3. Monthly PSC occurrence (%) for (a) 2006 and (b) 2007.

persist for a long time. However, these PSCs tend to be quasi-stationary relative to the mean stratospheric flow [Cariolle *et al.*, 1989]. As a result, mountain wave effects alone cannot explain this observed monthly and interannual spatial variability in PSC occurrence.

[16] Wang *et al.* [2008] showed that mesoscale tropospheric dynamics associated with deep tropospheric cloud systems have a significant impact on Antarctic PSC distribution. The Marie Byrd region, along with the Antarctic Peninsula and the continental region east of the Weddell Sea, has the highest PSC occurrence rates. These localized regions of high PSC occurrence rates lie in the downwind regions of intense mesoscale cyclogenesis in the Antarctic [Simmonds and Keay, 2000; Carrasco *et al.*, 2003]. Deep tropospheric clouds indicate the presence of large-scale lifting and cyclonic activities. Quasi-adiabatic uplift associated with these deep clouds can lower the temperature of the lower stratosphere, thereby increasing the possibility of PSC formation [Teitelbaum *et al.*, 2001]. However, for some specific regions, mountain waves may still be important for local PSC formation. Mountain waves may also affect downwind PSC formation by providing nuclei. In many cases, tropospheric mesoscale dynamical systems could couple with mountain waves to affect PSC formation.

[17] Figures 4a and 4b show the time-height distribution of PSC occurrence for 2006 and 2007, and Figure 4c shows the daily mean and minimum temperatures of the whole region to the south of 60°S at the 46 hPa (~20 km) level based on MLS measurements. The evolution of the PSCs in the region closely follows the evolution of the lower stratospheric temperature. The stratospheric temperature gradually decreased beginning in early May. By the fourth week of May, the mean temperature of the region south of 60°S dropped below 200 K above the 20 km level in 2006, with temperatures as low as 190 K in most of the interior continental region. During the same period in 2007, the mean temperature south of 60°S dropped below 195 K for altitudes above the 20 km level, with the interior region recording temperatures of 185–190 K at the 16 to 22 km levels. The first occurrence of PSCs commenced by the middle of the fourth week in May of 2007, starting between 20 and 25 km. The relationship between the onset of PSCs

in the Antarctic stratosphere and the evolution of synoptic-scale temperature indicates that wintertime cooling within the polar vortex is the major factor in the formation of PSCs over the Antarctic region in the early PSC season. Data for the 2006 season are only available after 15 June, so the evolution of PSCs during late May and early June could not

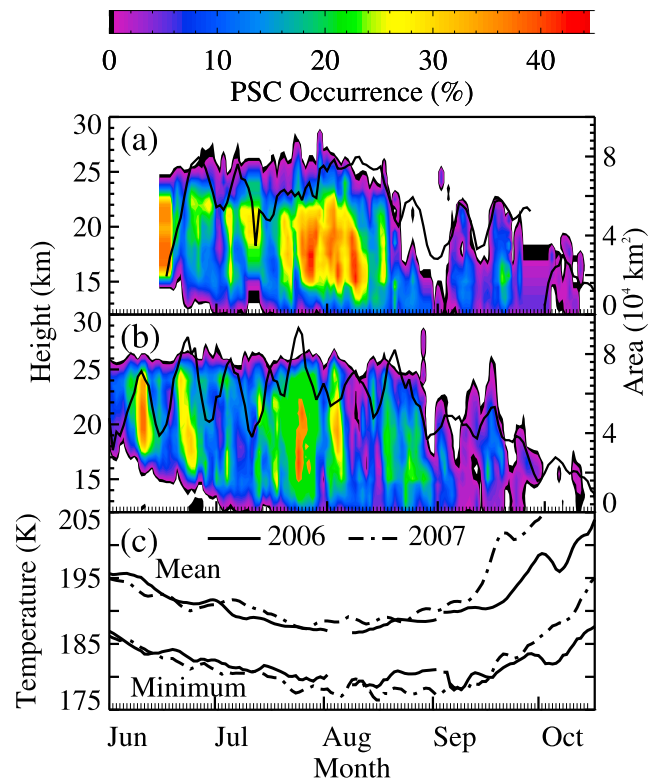


Figure 4. Distribution of PSCs: (a) 2006 and (b) 2007 daily vertical distribution of PSC occurrences. The solid black lines show the daily tropospheric cloud area (of high and deep clouds) in the vertical cross section under the satellite track. (c) Daily variation of mean and minimum temperature at 46 hPa (~20 km) for the region south of 60°S.

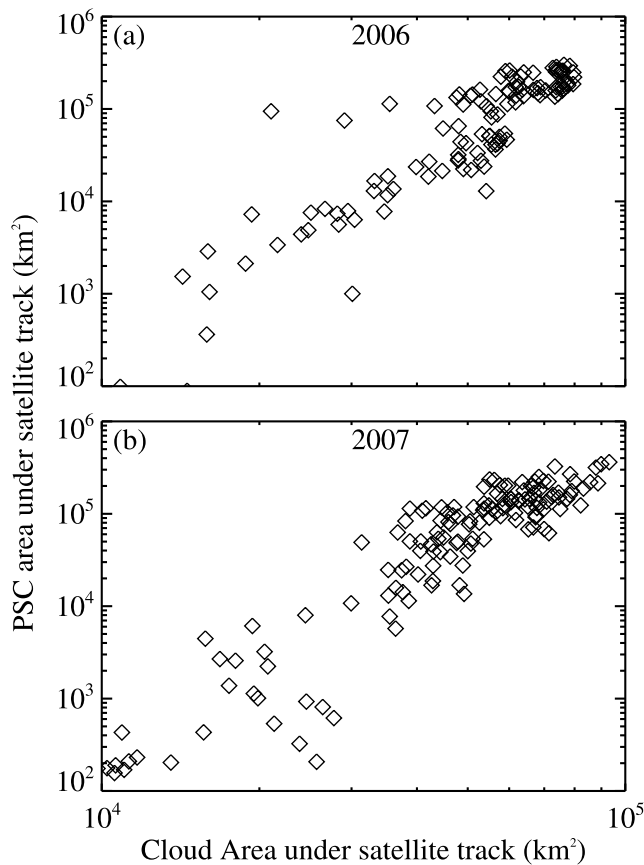


Figure 5. Scatterplot of cross-sectional areas under satellite track for PSCs and tropospheric clouds for (a) 2006 and (b) 2007. Tropospheric clouds include high and deep clouds.

be analyzed. In the early part of the season, PSCs form around an altitude of 20 km. The most frequent PSC occurrences are observed at altitudes of 18–24 km, which is consistent with the results obtained by *Adriani et al.* [2004]. During early July, frequent PSC occurrences are observed as low as 14 km, but the most frequent occurrences are still in the altitude range of 18–24 km. By late July and early August, PSCs occur at relatively low altitudes, with a maximum around 14–18 km; however, PSCs are still observed up to 25 km. During late August and most of September, most of the PSCs are confined to the lower stratosphere in the altitude range of 12–16 km.

[18] Large-scale temperature fields alone do not adequately explain the cell structure of PSC occurrence observed in the time-height plots of Figure 4. High PSC occurrence rates closely follow tropospheric cloudiness. Figures 4a and 4b also show the vertical cross-sectional area of deep tropospheric clouds along the satellite tracks. Higher PSC occurrences are observed when the tropospheric high and deep cloudiness increases. Figure 5 shows the scatterplot of the daily total vertical cross-sectional area along the satellite track for tropospheric high and deep clouds and PSCs. Pearson's correlation coefficients for these clouds are 0.78 and 0.79 for the 2006 and 2007 seasons, respectively. Figure 6a shows a 15 day running average for the percentage of PSCs

(in terms of vertical cross-sectional area) directly associated with deep tropospheric cloud systems. It is clear that the percentage statistically increases with time, and between 60 and 70% of the PSCs are associated with tropospheric cloud systems in the late part of the PSC season (late September). The daily mean ALSR (Figure 6b) is well correlated with the total vertical cross-sectional area of deep tropospheric cloud systems.

[19] Figure 6c shows that the areal coverage of the PSC systems increases from the start of the PSC season until late July/early August and decreases sharply thereafter. In 2007, the maximum PSC area was observed during the last week of July, whereas the maximum area in 2006 occurred during the first week of August. The mean stratospheric temperatures increased significantly during 2007 from the second week of September and exceeded 200 K at all levels within 15–25 km by the fourth week of September. Warming of the stratosphere causes significant reduction in PSC coverage, which decreases by more than 2 orders of magnitude by late September as compared with the peak value. The temperature rise in 2006 did not occur as rapidly as in 2007, and the mean stratospheric temperatures remained below 200 K until early October. A larger PSC areal coverage is observed in the later part of the PSC season in 2006 as compared to 2007. During the later part of the PSC season, PSCs are mostly confined to the coastal western Antarctic (30°W–130°W), a region of intense cyclogenesis. The role of localized cooling becomes more important as synoptic-scale temperatures rise above the temperatures required for PSCs. The increase in the fraction of PSCs associated with tropospheric clouds (60–70%) by early September during both years indicates the important role of tropospheric weather systems in PSC formation during the later PSC season.

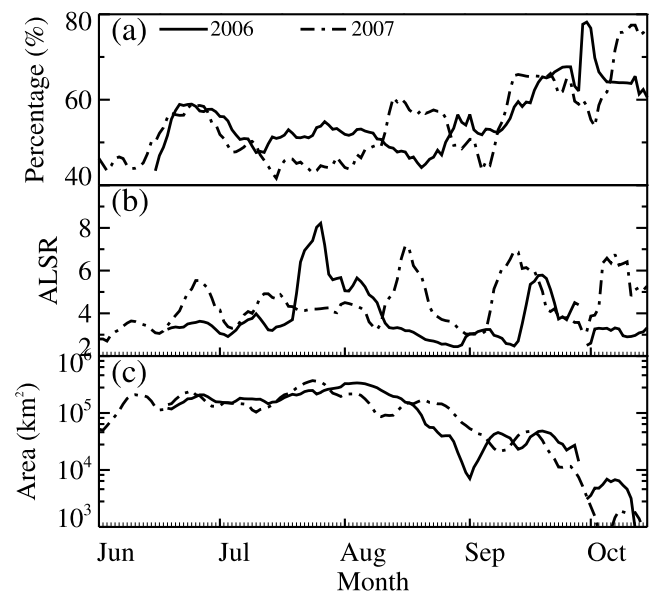


Figure 6. Mean daily variations of (a) percentage of PSCs (in area) associated with high and deep tropospheric cloud systems, (b) daily mean of ALSR for 2006 and 2007, and (c) PSC area in the vertical cross section along satellite track.

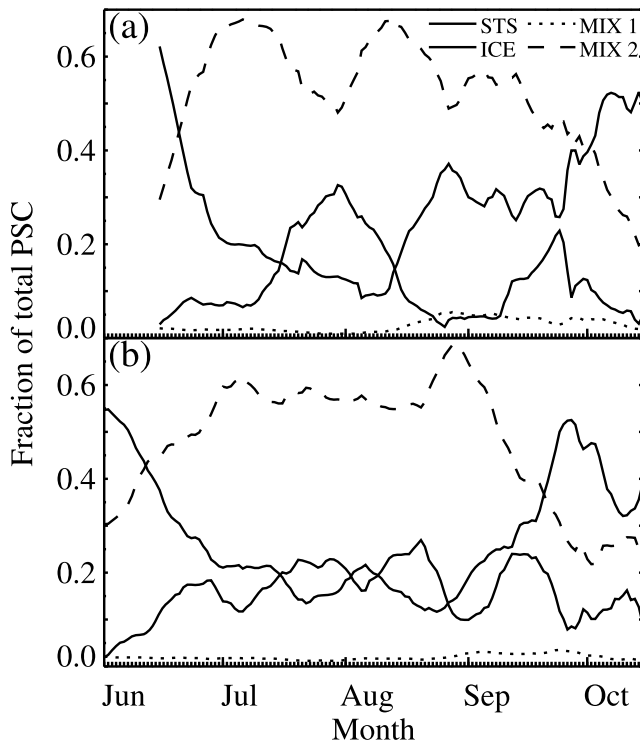


Figure 7. Daily variation of PSC classes for (a) 2006 and (b) 2007.

3.2. PSC Microphysical Properties and Their Dependence on Tropospheric Clouds

[20] In section 3.1, we showed that tropospheric high and deep cloud systems affect PSC occurrence, PSC areal coverage and the in-cloud ALSR distribution. Cooling associated with the presence of tropospheric clouds also has an impact on the microphysical properties of PSCs.

[21] Figure 7 shows the daily variation of different PSC compositions for the 2006 and 2007 seasons. The vertical axis shows the fractions for each PSC class. Figure 7 shows that more than 50% of PSCs are STS in the early season for both 2006 and 2007. The STS fraction drops sharply and reaches around 20% by late June. The relative fraction of the PSC classes Mix 2 and ice increases, while the STS fraction decreases. The increase in Mix 2 indicates that the mixtures containing crystalline particles (mostly NAT) increase. An increase in the depolarization signal shows that the optical properties of the mixture are influenced by the presence of crystalline particles. It indicates that the number concentration and/or size of the crystalline particles start to increase after the onset of PSC formation. The formation of ice crystals requires a reduction in temperature below the frost point, typically below 190 K. As the temperature drops with time from the onset of PSCs in late May/early June, ice crystals begin to appear. The fraction of the ice PSC class in the PSCs is small in the beginning of the PSC season and shows a large variation over the PSC season.

[22] Figure 8 shows the monthly mean distribution of the four PSC composition classes for June through October of 2006 (Figure 8a) and 2007 (Figure 8b) for PSCs associated

and not associated with tropospheric clouds separately. It is clear that there are similar numbers of observations associated with and not associated with tropospheric clouds in the early part of the PSC season. During the later part of the PSC season (September and October), however, most of the observed PSCs are associated with tropospheric clouds, especially for Mix 2 and ice. The effect of tropospheric high and deep cloud systems is more evident in the occurrence of ice PSCs. All five months of the PSC season in 2006 and 2007 show a higher occurrence of PSC ice for PSCs associated with tropospheric cloud systems. During the later part of the PSC season, when the stratosphere starts to warm up, more than 80% of the ice PSCs are associated with tropospheric cloud systems.

[23] During September and October, the stratospheric temperature starts to increase and ozone depletion is more active. PSC formation due to additional cooling provided by

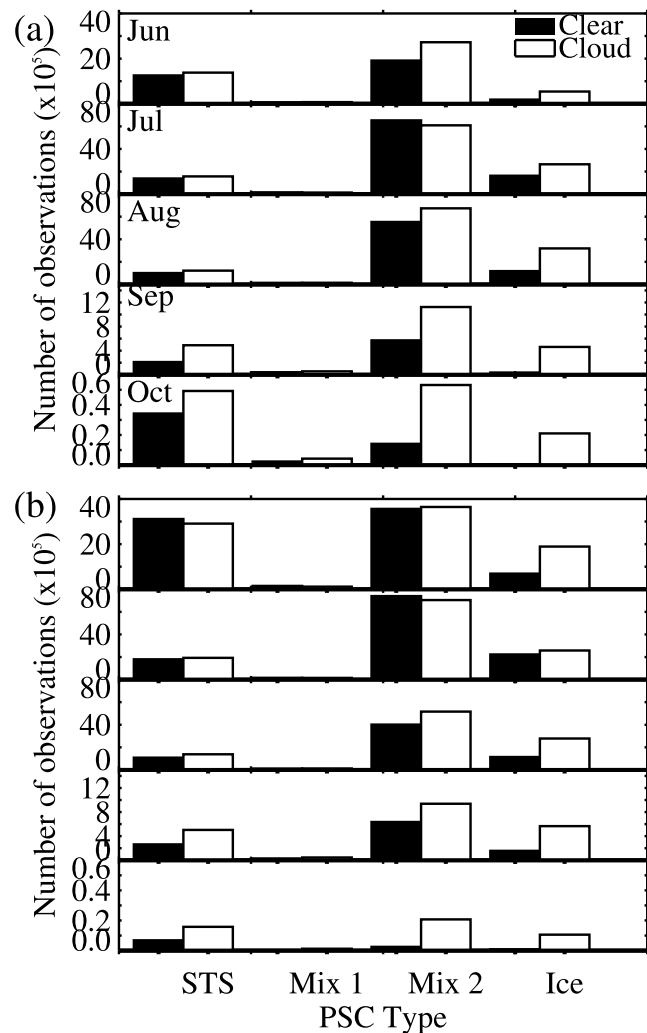


Figure 8. Histograms showing monthly distribution of observed occurrence of different types of PSCs for (a) 2006 and (b) 2007. Data for June 2006 are available only from 15 June, so June 2006 has a smaller number of observations than June 2007 for all PSC types.

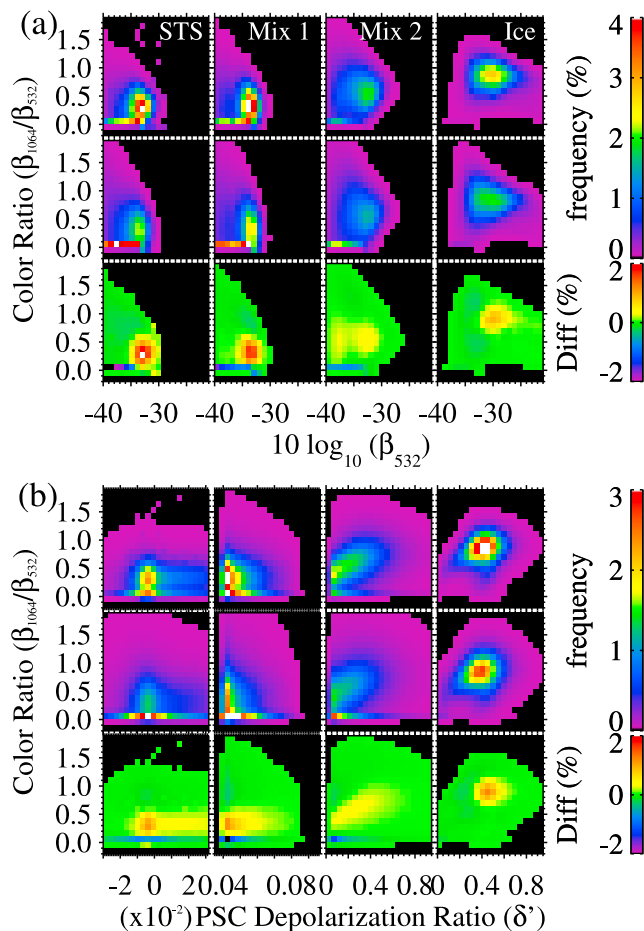


Figure 9. (a) Variation of color ratio (β_{1064}/β_{532}) and $10 \log_{10} \beta$ (backscattering coefficient, $\text{km}^{-1} \text{sr}^{-1}$) for STS, Mix 1, Mix 2, and ice PSCs from June through September of (top) 2006 and (middle) 2007. (b) Variation of color ratio and depolarization ratio (δ') for STS, Mix 1, Mix 2, and ice PSCs from June through September of (top) 2006 and (middle) 2007. The bottom plots in Figures 9a and 9b show the frequency difference between 2006 and 2007 (2006–2007).

the tropospheric cloud systems could be critical for ozone hole evolution.

3.3. PSC Microphysical Properties and Tropospheric Cloud Systems

[24] The microphysical properties of different classes of PSCs are analyzed based on their depolarization ratio, color ratio and backscattering coefficients. Figure 9 shows the frequency distribution of the four classes of PSCs in 2-D space: color ratio versus PSC depolarization ratio and color ratio versus backscattering coefficient.

[25] STS particles grow by condensational growth of nitric acid and water vapors on supercooled stratospheric aerosols, which are mostly sulfuric acid–water solutions [Tolbert, 1994, 1996; Zink *et al.*, 2002], and grow to sizes smaller than $1 \mu\text{m}$ [Toon *et al.*, 1990]. Hence, they are characterized by very low depolarization ratio and color ratio values. Figure 9

shows that the color ratio values for STS lie below 0.8, with the majority of the values between 0 and 0.5. Mix 1 and Mix 2 classes of PSCs contain mixtures of STS and crystalline NAT particles, which causes the depolarization ratio of the mixtures to be much larger than that of the STS class. Our choice of ALSR threshold and classification scheme limits the depolarization ratio for Mix 1 to less than 0.1, which indicates that Mix 1 is still dominated by STS. The similar distribution of STS and Mix 1 also confirms this. Due to the low signal-to-noise ratio for PSCs with low ALSRs, the estimated depolarization ratio could be negative. Mix 2 PSCs are dominated by NAT particles with color ratio values mainly within 0.4 and 1. The class of ice PSCs has depolarization values concentrated between 0.3 and 0.7, high color ratio values (within 0.5 and 1.4) and higher backscattering coefficients than the other three classes of PSCs.

[26] The 2006 and 2007 PSC seasons show several noticeable differences in PSC occurrence and properties. PSCs are observed in the early week of October in 2006, whereas they are almost absent by the end of September in 2007. The slightly colder temperatures within the polar vortex in 2006, together with additional cooling from tropospheric cloud systems, might be the cause of the persistence of PSCs until early October in 2006. In addition, more PSCs occurred at lower altitudes in 2006 than in 2007, which could indicate more efficient sedimentation of particles in 2006. Sedimentation of PSC particles results in the permanent removal of nitrogen compounds from the lower stratosphere. This denitrification of the lower stratosphere allows for ozone destruction by removing nitrogen compounds that convert chlorine radicals to reservoir species [Lowe and MacKenzie, 2008]. Total ozone maps obtained from Solar Backscattering Ultraviolet (SBUV/2) instruments aboard the National Oceanic and Atmospheric Administration (NOAA) polar orbiting satellites (www.cpc.ncep.noaa.gov/products/stratosphere/polar/polar.shtml) show a much larger ozone loss in the spring of 2006 than in the spring of 2007. The larger ozone loss observed in the early spring of 2006 might be related to greater denitrification and a longer persistence of PSCs in the 2006 season, in comparison to the 2007 season.

[27] According to Figure 8, high and deep tropospheric cloud systems significantly affect the relative occurrence of different PSC classes in September and October. As discussed above, different PSC classes have significant microphysical property differences. There are also noticeable microphysical property differences for the same class of PSCs associated and not associated with high and deep tropospheric cloud systems. Figure 10 shows the probability density functions (PDF) of backscattering coefficients and color ratios for the four PSC classes for the 2006 and 2007 seasons. We applied the *t* test to determine the statistical significance of whether the color ratio and backscattering coefficient of PSCs associated/not associated with tropospheric clouds have different means. Both the color ratios and the backscattering coefficients for the ice PSC class show significant differences between PSCs associated/not associated with tropospheric clouds at the 0.05 level, except in July. In the case of STS and Mix 1, the *t* test shows that there are no significant differences in the means of either the color ratio or the backscattering coefficient at the 0.05 level.

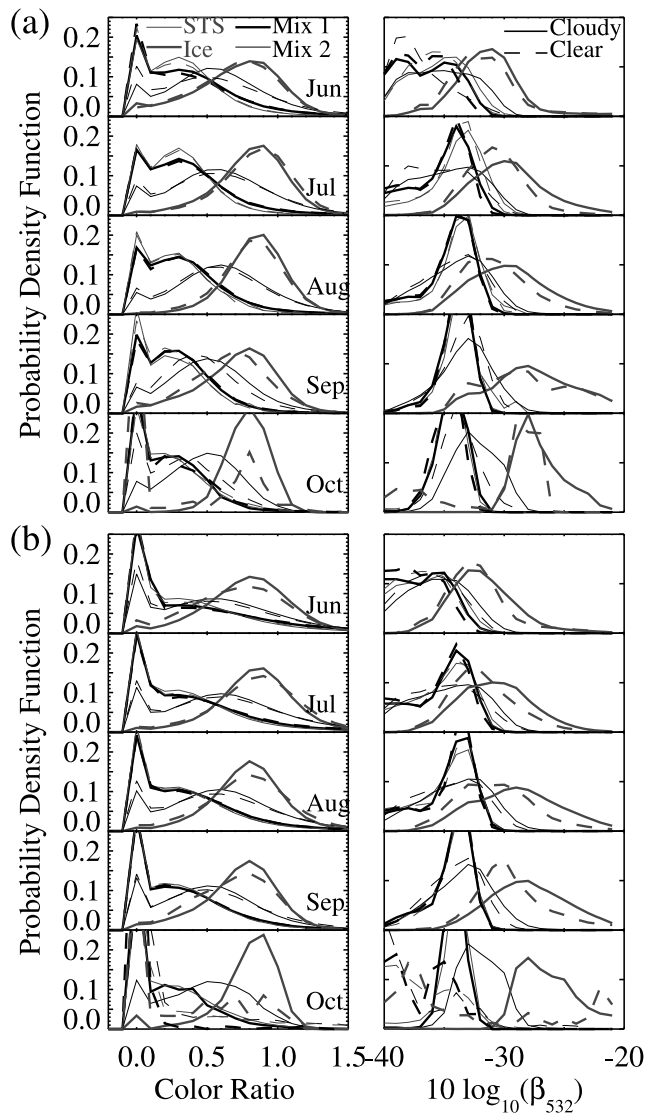


Figure 10. Probability density functions of color ratio (β_{1064}/β_{532} in left plots) and $10 \log_{10} \beta_{532}$ (backscattering coefficients, $\text{km}^{-1} \text{sr}^{-1}$ in right plots) from June through October for (a) 2006 and (b) 2007.

In the case of the Mix 2 class, significant differences (at the 0.05 level) exist for the late PSC seasons. Figure 10 also shows that high and deep tropospheric clouds have a smaller impact on the PSC color ratio than on the backscattering coefficient. The small impact on color ratios for each PSC class indicates that the effective particle size for each of the PSC classes is similar for PSCs associated and not associated with tropospheric clouds, except for ice and Mix 2 during October. In all four PSC classes, especially for Mix 2 and ice, PSCs associated with tropospheric clouds have larger backscattering coefficients than PSCs not associated with tropospheric clouds. A small change in color ratio accompanied by an increase in the backscattering coefficient indicates an increased PSC number concentration. Hence, PSCs associated with tropospheric clouds are more likely to have a higher number concentration than PSCs not associated with tropospheric clouds. A higher particle concentration

provides a larger surface area for stratospheric heterogeneous chemical reactions, leading to more ozone loss processes [Carslaw *et al.*, 1998].

4. Conclusion

[28] PSCs in the Antarctic region form in the polar winter night and remain until early October. Although cooling within the polar vortex is the main mechanism for the formation of PSCs, new NASA satellite data indicate that PSC occurrence and chemical and microphysical properties are also strongly associated with deep tropospheric cloud systems.

[29] The ALSR values from CALIPSO lidar measurements were used to identify PSCs, while combined CloudSat and CALIPSO data were used to identify tropospheric cloud systems. PSCs were classified into STS, Mix 1, Mix 2 and ice classes based on ALSR and PSC depolarization ratio values. The STS class is characterized by low color ratio values and values of backscattering coefficients (β) in the range of $0.0001\text{--}0.001 \text{ km}^{-1} \text{sr}^{-1}$, with a modal value of $0.0005 \text{ km}^{-1} \text{sr}^{-1}$. Mix 1 and Mix 2, which contain crystalline particles (mostly NAT) and STS, have a larger color ratio and larger depolarization ratio values than STS. The backscattering coefficients show modal values of 0.0004 and $0.0005 \text{ km}^{-1} \text{sr}^{-1}$ for Mix 1 and Mix 2, respectively. PSC ice has the largest color ratio values and the largest backscattering coefficients (modal value of $0.001 \text{ km}^{-1} \text{sr}^{-1}$). In the early part of the PSC season, PSCs are mainly distributed within altitudes of 18–25 km with dominant STS and gradually extend to lower altitudes with more frequent NAT and STS mixtures and ice particles. By mid-September, PSCs are mostly confined below 20 km, and they dissipate completely by early/mid October. The highest PSC occurrences in terms of areal coverage under the satellite track are observed during late July/early August. There are noticeable differences in the vertical PSC distributions and the temporal evolution of PSC classes between 2006 and 2007.

[30] Although PSCs are ubiquitous in the region, localized high PSC occurrence areas are present, which indicates the role of mesoscale dynamics in PSC formation. Topographically forced mountain waves are known to be important phenomena in PSC formation by adiabatically cooling the stratosphere and by providing nuclei; however, the significant variations observed in the high PSC occurrence regions among different months and between 2006 and 2007 indicate that mountain waves are not the major factor controlling PSC formation and distribution in the Antarctic region. Frequent PSC occurrences are observed in the regions downwind of high synoptic and mesoscale cyclonic activities as indicated by high and deep tropospheric cloud systems. Deep tropospheric clouds provide additional cooling in the low stratosphere, favoring PSC formation [Teitelbaum *et al.*, 2001; Wang *et al.*, 2008]. The correlation coefficients between PSC occurrence (%) and high and deep tropospheric cloud cross-sectional areas (under the satellite track) are 0.78 and 0.79 for 2006 and 2007, respectively. During the late PSC season, close to 70% of PSCs are formed in association with high and deep tropospheric cloud systems, indicating the important role of tropospheric weather systems in Antarctic PSC formation during the later PSC season. However, in many cases, tropospheric mesoscale dynamical systems could couple with mountain waves to affect PSC

formation, and mountain waves may still have a dominant role in PSC formation over some specific regions.

[31] Tropospheric cloud systems also affect the microphysical properties of PSCs. First, high and deep tropospheric cloud systems affect the relative occurrence of different PSC classes, especially during September and October; each PSC class has significantly different microphysical properties. Second, there are noticeable microphysical property differences (at the 0.05 significance level) between ice class and Mix 2 (late season only) associated and not associated with high and deep tropospheric cloud systems. For each PSC class (especially for Mix 2 and ice), those associated with tropospheric clouds have larger backscattering ratios than those not associated with tropospheric clouds; however, the difference in the color ratio is smaller. These observations suggest that the number concentration of PSC particles in each PSC class is larger when they are associated with tropospheric cloud systems. This indicates an increased nucleation efficiency, providing a higher number concentration in the presence of tropospheric clouds beneath PSCs. PSCs with a higher number concentration and similar size result in a large surface area per volume to support the heterogeneous chemistry responsible for ozone hole formation. The effect of tropospheric cloud systems is more evident for the ice PSCs. Ice particle formation requires a lower temperature than STS and NAT, so additional cooling provided by tropospheric cloud systems is more important. Both the 2006 and 2007 results show a higher occurrence of ice PSCs associated with cloud systems. During the late part of the PSC season, when the stratospheric temperatures are warmer, more than 80% of the ice PSCs are associated with tropospheric cloud systems.

[32] The strong association between tropospheric clouds and PSC occurrence, especially during the later part of the PSC season, indicates that the interaction between tropospheric meteorology and PSC should be better characterized to understand interannual ozone hole variations and ozone hole recovery. Detailed studies, however, are needed to further understand how different scale dynamics and complex terrain interactions generate strong tropospheric disturbances over Antarctica to fully represent PSCs in models.

[33] **Acknowledgments.** This research was funded by NASA grant NNX07AQ83G. Many thanks go to CALIPSO PIs Dave Winkler and Charles Trepte, CloudSat PIs Graeme Stephens and Deborah Vane, and the CALIPSO/CloudSat data group. We are also grateful to the anonymous reviewers whose comments led to improvements in this paper.

References

- Adriani, A., P. Massoli, G. Di Donfrancesco, F. Cairo, M. L. Moriconi, and M. Snels (2004), Climatology of polar stratospheric clouds based on lidar observations from 1993 to 2001 over McMurdo Station, Antarctica, *J. Geophys. Res.*, *109*, D24211, doi:10.1029/2004JD004800.
- Benson, C. M., K. Drdla, G. E. Nedoluha, E. P. Shettle, and K. W. Hoppel (2006), Polar stratospheric clouds in the 1998–2003 Antarctic vortex: Microphysical modeling and Polar Ozone and Aerosol Measurement (POAM) III observations, *J. Geophys. Res.*, *111*, D18206, doi:10.1029/2005JD006948.
- Browell, E., C. Butler, S. Ismail, P. Robinette, A. Carter, N. Higdon, O. Toon, M. Schoeberl, and A. Tuck (1990), Airborne lidar observations in the wintertime Arctic stratosphere: Polar stratospheric clouds, *Geophys. Res. Lett.*, *17*(4), 385–388, doi:10.1029/GL017i004p00385.
- Cariolle, D., S. Muller, and F. Cayla (1989), Mountain waves, polar stratospheric clouds, and the ozone depletion over Antarctica, *J. Geophys. Res.*, *94*(D9), 11,233–11,240, doi:10.1029/JD094iD09p11233.
- Carrasco, K. F., D. H. Bromwich, and A. J. Monaghan (2003), Distribution and characteristics of mesoscale cyclones in the Antarctic: Ross Sea eastward to the Weddell Sea, *Mon. Weather Rev.*, *131*, 289–301, doi:10.1175/1520-0493(2003)131<0289:DACOMC>2.0.CO;2.
- Carslaw, K. S., B. P. Luo, S. L. Clegg, T. Peter, P. Brimblecombe, and P. J. Crutzen (1994), Stratospheric aerosol growth and HNO₃ gas phase depletion from coupled HNO₃ and water uptake by liquid particles, *Geophys. Res. Lett.*, *21*(23), 2479–2482, doi:10.1029/94GL02799.
- Carslaw, K. S., et al. (1998), Increased stratospheric ozone depletion due to mountain-induced atmospheric waves, *Nature*, *391*, 675–678, doi:10.1038/35589.
- Chu, L. T., M.-T. Leu, and L. F. Keyser (1993), Heterogeneous reactions of HOCl + HCl → Cl₂ + H₂O and ClONO₂ + HCl → Cl₂ + HNO₃ on ice surfaces at polar stratospheric conditions, *J. Phys. Chem.*, *97*, 12,798–12,804, doi:10.1021/j100151a028.
- Del Negro, L. A., et al. (1997), Evaluating the role of NAT, NAD, and liquid H₂SO₄/H₂O/HNO₃ solutions in Antarctic polar stratospheric cloud aerosol: Observations and implications, *J. Geophys. Res.*, *102*(D11), 13,255–13,282, doi:10.1029/97JD00764.
- Dougllass, A. R., R. S. Stolarski, S. E. Strahan, and B. C. Polansky (2006), Sensitivity of Arctic ozone loss to polar stratospheric cloud volume and chlorine and bromine loading in a chemistry and transport model, *Geophys. Res. Lett.*, *33*, L17809, doi:10.1029/2006GL026492.
- Drdla, K., A. Tabazadeh, R. P. Turco, M. Z. Jacobson, J. E. Dye, C. Twohy, and D. Baumgardner (1994), Analysis of the physical state of one Arctic polar stratospheric cloud based on observations, *Geophys. Res. Lett.*, *21*(23), 2475–2478, doi:10.1029/94GL02405.
- Fahey, D. W., et al. (2001), The detection of larger HNO₃-containing particles in the winter Arctic stratosphere, *Science*, *291*, 1026–1031, doi:10.1126/science.1057265.
- Fromm, M. D., J. D. Lumpe, R. M. Bevilacqua, E. P. Shettle, J. Hornstein, S. T. Massie, and K. H. Fricke (1997), Observations of Antarctic polar stratospheric clouds by POAM II: 1994–1996, *J. Geophys. Res.*, *102*(D19), 23,659–23,672, doi:10.1029/97JD00794.
- Fromm, M. D., R. M. Bevilacqua, J. Hornstein, E. Shettle, K. Hoppel, and J. D. Lumpe (1999), An analysis of Polar Ozone and Aerosol Measurement (POAM) II arctic polar stratospheric cloud observation, 1993–1996, *J. Geophys. Res.*, *104*(D20), 24,341–24,357, doi:10.1029/1999JD900273.
- Fromm, M., J. Alfred, and M. Pitts (2003), A unified, long-term, high-latitude stratospheric aerosol and cloud database using SAM II, SAGE II, and POAM II/III data: Algorithm description, database definition, and climatology, *J. Geophys. Res.*, *108*(D12), 4366, doi:10.1029/2002JD002772.
- Gobbi, G. P., G. D. Donfrancesco, and A. Adrini (1998), Physical properties of stratospheric clouds during the Antarctic winter of 1995, *J. Geophys. Res.*, *103*(D9), 10,859–10,873, doi:10.1029/98JD00280.
- Hanson, D., and K. Mauersberger (1988), Laboratory studies of the nitric acid trihydrate: Implications for the south polar stratosphere, *Geophys. Res. Lett.*, *15*(8), 855–858, doi:10.1029/GL015i008p00855.
- Hopfner, M., B. P. Luo, P. Massoli, R. Spang, M. Snels, G. Di Donfrancesco, G. Stiller, T. Von Clarmann, H. Fischer, and U. Biermann (2006), Spectroscopic evidence for NAT, STS, and ice in MIPAS infrared limb emission measurements of polar stratospheric clouds, *Atmos. Chem. Phys.*, *6*, 1201–1219.
- Jensen, E. J., O. B. Toon, A. Tabazadeh, and K. Drdla (2002), Impact of polar stratospheric cloud particle composition, number density, and lifetime on denitrification, *J. Geophys. Res.*, *107*(D20), 8284, doi:10.1029/2001JD000440.
- Larsen, N., I. S. Mikkelsen, B. M. Knudsen, J. Schreiner, C. Voigt, K. Mauersberger, J. M. Rosen, and N. T. Kjome (2000), Comparison of chemical and optical in situ measurements of polar stratospheric cloud particles, *J. Geophys. Res.*, *105*(D1), 1491–1502, doi:10.1029/1999JD900910.
- Lowe, D., and A. R. MacKenzie (2008), Polar stratospheric cloud microphysics and chemistry, *J. Atmos. Sol. Terr. Phys.*, *70*, 13–40.
- Noel, V., A. Hertzog, H. Chepfer, and D. M. Winker (2008), Polar stratospheric clouds over Antarctica from the CALIPSO spaceborne lidar, *J. Geophys. Res.*, *113*, D02205, doi:10.1029/2007JD008616.
- Pitts, M. C., L. W. Thomason, L. R. Poole, and D. M. Winker (2007), Characterization of polar stratospheric clouds with space-borne lidar: CALIPSO and the 2006 Antarctic season, *Atmos. Chem. Phys. Discuss.*, *7*, 7933–7985.
- Pitts, M. C., L. R. Poole, and L. W. Thomason (2009), CALIPSO polar stratospheric cloud observations: Second generation detection algorithm and composition discrimination, *Atmos. Chem. Phys. Discuss.*, *9*, 8121–8157.
- Rex, M., R. J. Salawitch, P. von der Gathen, N. R. P. Harris, M. P. Chipperfield, and B. Naujokat (2004), Arctic ozone loss and climate change, *Geophys. Res. Lett.*, *31*, L04116, doi:10.1029/2003GL018844.

- Simmonds, I., and K. Keay (2000), Mean Southern Hemisphere extratropical cyclone behavior in the 40-year NCEP-NCAR reanalysis, *J. Clim.*, *13*, 873–885, doi:10.1175/1520-0442(2000)013<0873:MSHECB>2.0.CO;2.
- Solomon, S. (1999), Stratospheric ozone depletion: A review of concepts and history, *Rev. Geophys.*, *37*, 275–316, doi:10.1029/1999RG900008.
- Spang, R., J. J. Remedios, L. J. Kramer, L. R. Poole, M. D. Fromm, G. Baumgarten, and P. Konopka (2005), Polar stratospheric clouds observations by MIPAS on ENVISAT: Detection method, validation and analysis of the Northern Hemisphere winter 2002/2003, *Atmos. Chem. Phys.*, *5*, 679–692.
- Stephens, G. L., et al. (2002), The CloudSat mission and the A-Train, *Bull. Am. Meteorol. Soc.*, *83*, 1771–1790, doi:10.1175/BAMS-83-12-1771.
- Strawa, A. W., K. Drdla, M. Fromm, R. F. Pueschel, K. W. Hoppel, E. V. Browell, P. Hamill, and D. P. Dempsey (2002), Discriminating Types Ia and Ib polar stratospheric clouds in POAM satellite data, *J. Geophys. Res.*, *107*(D20), 8291, doi:10.1029/2001JD000458.
- Svensen, S. H., N. Larsen, B. Knudsen, S. D. Eckermann, and E. V. Browell (2005), Influence of mountain waves and NAT nucleation mechanism on polar stratospheric cloud formation at local scales during the 1999–2000 Arctic winter, *Atmos. Chem. Phys.*, *5*, 739–753.
- Tabazadeh, A., P. Turco, K. Drdla, M. Z. Jacobson, and O. B. Toon (1994), A study of Type 1 polar stratospheric cloud formation, *Geophys. Res. Lett.*, *21*(15), 1619–1622, doi:10.1029/94GL01368.
- Tabazadeh, A., S. T. Martin, and J.-S. Lin (2000), The effect of particle size and nitric acid uptake on the homogeneous freezing of aqueous sulfuric acid particles, *Geophys. Res. Lett.*, *27*(8), 1111–1114, doi:10.1029/1999GL010966.
- Tabazadeh, A., E. J. Jensen, O. B. Toon, K. Drdla, and M. R. Schoeberl (2001), Role of stratospheric polar freezing belt in denitrification, *Science*, *291*, 2591–2594, doi:10.1126/science.1057228.
- Teitelbaum, H., M. Moustouli, and M. Fromm (2001), Exploring polar stratospheric cloud and ozone minihole formation: The primary importance of synoptic-scale flow perturbation, *J. Geophys. Res.*, *106*(D22), 28,173–28,188, doi:10.1029/2000JD000065.
- Tolbert, M. A. (1994), Sulfate aerosols and polar stratospheric cloud formation, *Science*, *264*, 527–528, doi:10.1126/science.264.5158.527.
- Tolbert, M. A. (1996), Polar clouds and sulfate aerosols, *Science*, *272*, 1597, doi:10.1126/science.272.5268.1597.
- Tolbert, M. A., and O. B. Toon (2001), Solving the PSC mystery, *Science*, *292*, 61–63, doi:10.1126/science.1060083.
- Toon, O. B., E. V. Browell, S. Kinne, and J. Jordan (1990), An analysis of lidar observations of polar stratospheric clouds, *Geophys. Res. Lett.*, *17*(4), 393–396, doi:10.1029/GL017i004p00393.
- Voigt, C., et al. (2000), Nitric acid trihydrate (NAT) in polar stratospheric clouds, *Science*, *290*, 1756–1758, doi:10.1126/science.290.5497.1756.
- Wang, Z., G. Stephens, T. Deshler, C. Trepte, T. Parish, D. Vane, D. Winker, D. Liu, and L. Adhikari (2008), Association of Antarctic polar stratospheric cloud formation on tropospheric cloud systems, *Geophys. Res. Lett.*, *35*, L13806, doi:10.1029/2008GL034209.
- Winker, D. M., J. R. Pelon, and M. P. McCormick (2003), The CALIPSO mission: Spaceborne lidar for observation of aerosols and clouds, *Proc. SPIE Int. Soc. Opt. Eng.*, *4893*, 1–11, doi:10.1117/12.466539.
- World Meteorological Organization (2007), Scientific assessment of ozone depletion: 2006, *Global Ozone Res. Monit. Proj. Rep. 50*, 572 pp., Geneva.
- Worsnop, D. R., L. E. Fox, M. S. Zahniser, and S. C. Wofsy (1993), Vapor pressure of solid hydrates of nitric acid: Implications for polar stratospheric clouds, *Science*, *259*, 71–74, doi:10.1126/science.259.5091.71.
- Zink, P., D. A. Knopf, J. Schreiner, K. Mauersberger, O. Möhler, H. Saathoff, M. Seifert, R. Tiede, and U. Schurath (2002), Cryo-chamber simulation of stratospheric H₂SO₄/H₂O particles: Composition analysis and model comparison, *Geophys. Res. Lett.*, *29*(11), 1551, doi:10.1029/2001GL013296.

L. Adhikari, D. Liu, and Z. Wang, Department of Atmospheric Science, University of Wyoming, 1000 E. University Ave., Laramie, WY 82071, USA. (zwang@uwyo.edu)